JGS
Journal of the Geological Society

Research Article

Published Online First

doi:10.1144/jgs2016-010

Geodynamics of Late Carboniferous–Early Permian forearc in north Chile (28°30′–29°30′S)

C. Creixell[1]*, V. Oliveros[2], P. Vásquez[1], J. Navarro[3], D. Vallejos[2], X. Valin[2], E. Godoy[4] & M. N. Ducea[5,6]

[1] Servicio Nacional de Geología y Minería, Avenida Santa María 0104, Providencia, Santiago, Chile
[2] Departamento Ciencias de la Tierra, Universidad de Concepción, Barrio Universitario s/n, Concepción, Chile
[3] Departamento de Geología, Universidad de Chile, Plaza Ercilla 803, Santiago, Chile
[4] Tehema Consultores Geológicos, Virginia Subercaseaux 4100, Pirque, Santiago, Chile
[5] Department of Geosciences, University of Arizona, Tucson, AZ 85721, USA
[6] Universitatea Bucaresti, Facultatea de Geologie Geofizica, Strada N. Balcescu Nr 1, Bucuresti, Romania
* Correspondence: christiancreixell@gmail.com

Abstract: A large section of the Late Palaeozoic forearc is exposed along the coastal ranges of north–central Chile (28°–29° 30′S). This is characterized by three lithotectonic units: (1) the Punta de Choros Metamorphic Complex (basal accretion series), composed mostly of micaschists and metabasites; (2) the Chañaral Epimetamorphic Complex (frontal accretion series), formed by metaturbidites and metasediments; (3) the Llano del Chocolate Beds (forearc basin deposits), composed of a sedimentary sequence of clastic sedimentary rocks with minor limestones and acidic volcanic rocks. Within the basal accretion series, two distinctive blocks of garnet-bearing schists with amphibolite-facies metamorphism have been preserved, recording early stages of the subduction system. The stratigraphic record and the U–Pb dating of igneous (291–318 Ma) and detrital zircons (maximal deposition ages between 273 and 292 Ma) in the forearc basin deposits, coupled with $^{40}Ar/^{39}Ar$ ages for metamorphic rocks (319–280 Ma), indicate that forearc sedimentation was broadly contemporaneous with metamorphism and exhumation of the basal accretion series. The radiometric dating on garnet-bearing rocks indicates that the onset of the subduction system took place in the Mississippian, at a high thermal gradient. These conditions were responsible for generation of limited volumes of acidic melt, now recognized as acidic domes and tuffs within the forearc basin stratigraphy.

Supplementary material: Tables of sedimentary facies, U-Pb geochronological analyses and Ar-Ar geochronological data are available at: https://doi.org/10.6084/m9.figshare.c.2868307.

Received 24 July 2015; **revised** 22 January 2016; **accepted** 22 February 2016

Accretionary forearcs along continental boundaries are key locations to understand the mechanics and thermodynamic evolution of subduction, as well as the processes of crustal construction and destruction along continental margins, as seismogenic deformation along thrust faults, fluid flow and mass transfer from the oceanic to the continental plate is occurring along these zones (Fisher 1996; Cloos & Schreve 1988; Moore *et al*. 2007; Mosher *et al*. 2008). The anatomy of an accretionary forearc consists basically of an outer ridge, an accretionary prism, forearc and trench slope basins (i.e. Stern 2002). Brittle to ductile deformation, largely concentrated along accretionary prisms, is dependent on several factors, such as pressure, temperature and fluid pressure (e.g. Peacock 1996). Direct observations of fossil basal zones of accretionary prisms and the zone of basal accretion crystallized along the subduction channel reveal complex processes of mass transfer between oceanic and continental plates. These processes are recorded in complex patterns of tectonic juxtaposition of slices of partially exhumed oceanic high-pressure rocks, metamorphosed under eclogite- and blueschist-facies conditions, along with shallower slices of metamorphosed sediments and volcanic rocks (Willner *et al*. 2004; Agard *et al*. 2009; Hyppolito *et al*. 2014).

Contemporaneously with development of accretionary prisms, forearc basins have been recognized that are located either above the deformation front or separated from the accretionary zone by a forearc high (e.g. Mosher *et al*. 2008). These forearc basins generally reveal a lower amount of strain and, when they are located on Andean-type active continental margins, their sediments are often derived from prevailing intracontinental environments. The geometry of the forearc basins could be controlled by thrust faults propagated from below the crust or even by extensional fractures, associated with exhumation of basal portions of the prism (e.g. Glodny *et al*. 2005; Willner *et al*. 2005). Also, in the Andean active continental margin large-scale dextral strike-slip faults, of presumable Triassic age, parallel to the continental margin, have been advocated as an important factor controlling the geometry and exhumation of forearc basins (Kato & Godoy 2015). At present, timescales linking processes of accretion and deformation along the prism and coupled evolution of forearc basins above it are poorly constrained. In this sense, the coastal range of north and central Chile, south of 27°S, is an exceptional site owing to the preservation and exposure of an ancient forearc system, which includes different levels of a Late Palaeozoic (Carboniferous–Permian) accretionary wedge with frontal and basal accretion series and coeval intracontinental forearc basins.

In this contribution we present a generalized geodynamic setting for the development of the Late Carboniferous–Early Permian forearc of north Chile at 29°–29°30′S, based on identification and mapping of several lithostructural associations of basal and frontal accretion metamorphic rocks and volcano-sedimentary successions of the forearc basin. The structure and age of crystallization of the metamorphic rocks are characterized by $^{40}Ar/^{39}Ar$ radiometric dating. For the sedimentary sequence of the forearc basin (Llano de Chocolate Beds), we present a complete stratigraphy and the interpretation of its sedimentary environment, coupled with U–Pb ages from detrital and igneous zircons, to determine the precise age

of sedimentation and exhumation and the provenance of material that filled the basin.

Geological setting

Late Palaeozoic geological evolution of the southwestern Gondwana margin

The Late Palaeozoic subduction along the western margin of Gondwana started around Mississippian times according to several researchers (e.g. Hervé 1988; Willner *et al*. 2004; Hervé *et al*. 2007; Hyppolito *et al*. 2014), following a stage of passive margin sedimentation in the Late Devonian–Early Carboniferous, represented by platform and turbiditic deposits in north Chile (Bahlburg & Hervé 1997; Augustsson *et al*. 2015). Most of this sedimentation probably occurred along the passive margin after collision of a suspected exotic terrane ('Chilenia') accreted to the continent during the Devonian (*c*. 390 Ma, Willner *et al*. 2011), whose collision vestiges are represented in western Argentina by the Guarguaráz complex (Massonne & Calderón 2008; Willner *et al*. 2011). After this collision, the onset of subduction occurred on the restored continental margin of western Gondwana. A different evolutionary model proposes that the Chilenia and Cuyania terranes were continental fragments separated by rifting (Davis *et al*. 2000) from a continental plate named Occidentalia during the Late Proterozoic (Dalla Salda *et al*. 1992). On one hand, collision of the eastern margin of Cuyania gave rise to the Famatinian collisional orogen in the Ordovician, and, on the other hand, final collision of the Chilenia terrane with the Gondwana continent resulted in the construction during the Early Carboniferous of the Chanic Orogen, which is now exposed in western Argentina (Heredia *et al*. 2014). In this sense, the Guarguaráz complex represents a slice of the accretionary complex of the Chanic subduction system emplaced over the eastern margin of the Chilenia terrane.

Renewed subduction was established on the western margin of Gondwana during the Late Carboniferous. Representative outcrops of accretionary prisms of this period are exposed continuously along the coast south of 34°S in a roughly NNW–SSE belt (Hervé 1988), to the west of and parallel to a continuous belt of a Late Carboniferous to Early Permian subduction-related batholiths, which has been interpreted as the intrusive product of the magmatic arc (Fig. 1a; Parada 1990; Lucassen *et al*. 2004; Deckart *et al*. 2014). Between 33° and 38°S, the metamorphic complexes consist mostly of two types of metamorphic associations: the Western Series of high *P*/*T* metamorphic gradient and the Eastern Series of low *P*/*T* metamorphic gradient (e.g. Hervé 1988). These associations were proposed as an example of paired metamorphic belts (Aguirre *et al*. 1972; Ernst 1975) that could characterize active subduction margins. In this model, the Eastern Series is affected by a higher thermal gradient at least in part related to the intrusion of the Late Palaeozoic batholith (Hervé 1977). The Western and Eastern Series have recently been associated with basal and frontal accretion zones, respectively, of accretionary prisms (Willner *et al*. 2004, 2005; Glodny *et al*. 2005).

Carboniferous to Permian accretionary prisms of north–central Chile (28°–31°S)

At 31°S, the outcrops representing Late Palaeozoic accretionary complexes are discontinuous. Prominent forearc associations are grouped in the Choapa Metamorphic Complex (Rebolledo & Charrier 1994), representative of basal accretion, and the Arrayán Formation, representative of frontal accretion series (Willner *et al*. 2008). Spatially related marine deposits of the Huentelauquén Formation have been interpreted as the material that filled the forearc or retro-wedge basin related to this Late Palaeozoic margin (Thiele & Hervé 1984; Willner *et al*. 2008). Farther north, between 26° and 29° S, an association of micaschists, greenschists and low-grade metasediments has been grouped in the Chañaral Epimetamorphic Complex (Godoy & Lara 1998), whereas between 29°00′ and 29° 30′S, similar metamorphic rocks are grouped in the Punta de Choros Metamorphic Complex (Creixell *et al*. 2012). Age constraints in the metamorphic rocks around 31°S indicate maximum depositional ages around 294–346 Ma for frontal accreted sediments, whereas the start of exhumation of basal accreted sediments from the subduction channel occurred at 307–274 Ma, probably extending to 242 Ma (Willner *et al*. 2012). According to Willner *et al*., frontal accretion and metamorphism occurred earlier than basal accretion, probably before 310 Ma. Further north, Bahlburg *et al*. (2009) obtained an Early Permian (294 Ma) maximum depositional age for the Huasco beds, part of the Chañaral Epimetamorphic Complex. On the other hand, Navarro (2013) reported a Mississippian maximum depositional age for micaschists exposed at 29°15′S, whereas Alvarez *et al*. (2011) obtained a maximum depositional age of 342 Ma for the same rocks. In contrast to the continuous outcrops south of 34°S, the Late Palaeozoic batholith is exposed as such (uninterrupted by younger rocks) at least 80 km east of forearc rocks. These granitoids are largely exposed along a north–south belt in the Frontal Cordillera, with several age peaks (324–316, 295–284 and 270–258 Ma; Salazar *et al*. 2013; Hervé *et al*. 2014; Maksaev *et al*. 2014), with the Early Permian peak (Chanchoquín Plutonic Complex) being volumetrically more significant (Salazar *et al*. 2013).

Analytical methods

A total of six samples were analysed for U–Pb geochronology. In three of these samples, corresponding to volcanic rocks from the Llano de Chocolate Beds, we obtained zircon crystallization ages. Furthermore, in three samples of sandstones from the same unit, we made detrital zircon age studies. We also present three new white mica and one biotite Ar–Ar ages, from samples of the Punta de Choros Metamorphic Complex, and we have reinterpreted three Ar–Ar ages, already published by Creixell *et al*. (2012), from one amphibole and two white mica samples belonging to the same unit.

Zircons were extracted from the rock samples by crushing, milling, gravitational separation and heavy liquids treatment. At least 50 crystals were randomly selected (regardless of their size, form or colour) using a stereomicroscope and then mounted in 25 mm epoxy and polished.

U–Pb geochronology of zircons was determined by laser ablation multicollector inductively coupled plasma mass spectrometry at the Arizona LaserChron Center (Gehrels *et al*. 2008). The analyses involved ablation of zircon with a New Wave/Lambda Physik DUV193 Excimer laser (operating at a wavelength of 193 nm) using a spot diameter of 25 or 35 mm. The ablated material was carried with helium gas into the plasma source of a GV Instruments Isoprobe equipped with a flight tube of sufficient width that U, Th and Pb isotopes were measured simultaneously. All measurements were made in static mode, using Faraday detectors for ^{238}U and ^{232}Th, an ion-counting channel for ^{204}Pb, and either Faraday collectors or ion counting channels for $^{208–206}$Pb. Ion yields were *c*. 1 mV ppm^{-1}. Each analysis consisted of one 20 s integration on peaks with the laser off (for backgrounds), twenty 1 s integrations with the laser firing, and a 30 s delay to purge the previous sample and to prepare for the next analysis. The ablation pit was *c*. 15 mm in depth.

For each analysis, the errors in determining ^{206}Pb/^{238}U and ^{206}Pb/^{204}Pb result in a measurement error of *c*. 1% (at 2σ level) in the ^{206}Pb/^{238}U age. The errors in measurement of ^{206}Pb/^{207}Pb and ^{206}Pb/^{204}Pb also result in *c*. 1% (2σ) uncertainty in age for grains that are >1.0 Ga, but are substantially larger for younger grains owing to low intensity of the ^{207}Pb signal. For most analyses, the

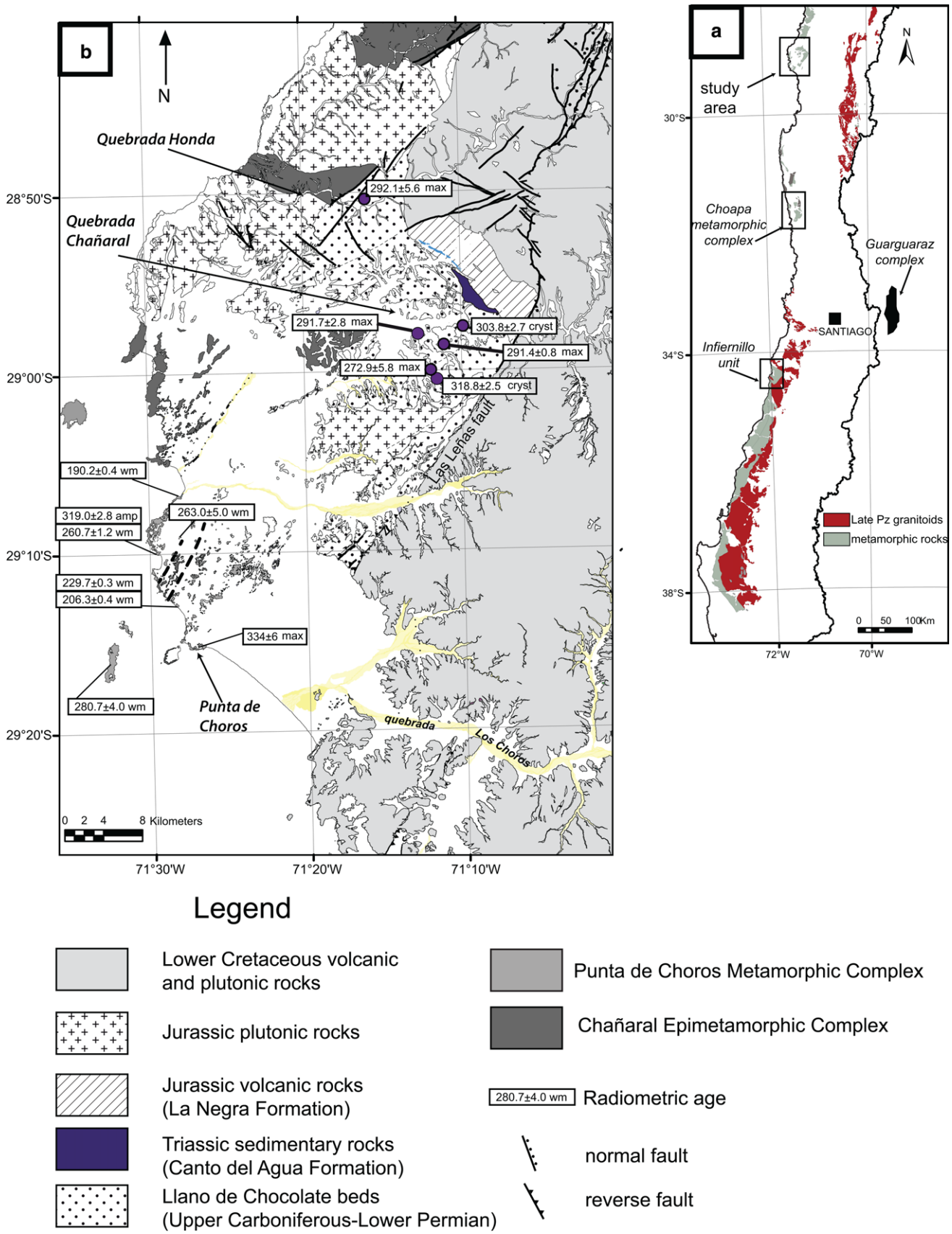

Fig. 1. (**a**) Geological map (modified from SERNAGEOMIN 2002) showing distribution of Late Palaeozoic metamorphic rocks and Late Palaeozoic granitoids in north–central Chile. Northern square indicates location of the study area. Location of the Guarguaraz Complex from Willner *et al*. (2011), Infiernillo Unit from Hyppolito *et al*. (2014) and Choapa Metamorphic Complex from Rebolledo & Charrier (1994) is also shown. (**b**) Geological map of the study area. Abbreviatures for radiometric ages: wm, Ar–Ar age on white mica; amp, Ar–Ar age on amphibole; max, U–Pb maximum depositional age on detrital zircons; cryst, U–Pb crystallization age on magmatic zircons.

crossover in precision of $^{206}Pb/^{238}U$ and $^{206}Pb/^{207}Pb$ ages occurs at *c*. 1.0 Ga. Common Pb correction was accomplished by using the measured ^{204}Pb and assuming an initial Pb composition from Stacey & Kramers (1975) (with uncertainties of 1.0 for $^{206}Pb/^{204}Pb$ and 0.3 for $^{207}Pb/^{204}Pb$). The measurement of ^{204}Pb is unaffected by the presence of ^{204}Hg because backgrounds are measured on peaks (thereby subtracting any background ^{204}Hg and ^{204}Pb), and because very little Hg is present in the argon gas. Interelement fractionation of Pb/U is generally *c*. 20%, whereas fractionation of Pb isotopes is generally <2%. In-run analysis of fragments of a large Sri Lankan zircon crystal (generally every fifth measurement) with known age of 564 ± 4 Ma (2σ error) was used to correct for this fractionation (see Gehrels *et al*. 2008). The uncertainty resulting from the calibration correction is generally *c*. 1% (2σ) for both $^{206}Pb/^{207}Pb$ and $^{206}Pb/^{238}U$ ages. The reported ages are determined from the weighted mean of the $^{206}Pb/^{238}U$ ages of the concordant and overlapping analyses (Ludwig 2003). The reported uncertainty (labelled 'mean') is based on the scatter and precision of the set of $^{206}Pb/^{238}U$ or $^{206}Pb/^{207}Pb$ ages, weighted according to their measurement errors (shown at 1σ). The systematic error, which includes contributions from the standard calibration, age of the calibration standard and composition of common Pb and U decay constants, is generally *c*. 1–2% (2σ).

The $^{40}Ar/^{39}Ar$ geochronological dating was carried out at the Isotope Geology Laboratory of SERNAGEOMIN on mineral separates of hornblende, biotite and white mica. Approximately 1 kg of sample was crushed and sieved to obtain grain sizes of 100–250 μm. Minerals were separated using an isodynamic Frantz magnetic separator and heavy liquids, followed by hand-picking under binocular microscope. Samples were mounted in high-purity Al discs (with space for 21 samples), together with sanidine crystals of Fish Canyon standard sample (28.02 ± 0.1 Ma; Renne *et al*. 1998). Samples were irradiated in a RECH-1 nuclear reactor at CCHEN (Comisión Chilena de Energía Nuclear, La Reina, Santiago) nuclear reactor facility for 22 h in a Herald-type pool, at 5 MW power energy. Samples inside the reactor were mounted in a stable and rotating position, surrounded by a Cd shell. The rotating system was used to obtain a homogeneous J factor for the various samples across the disk. After irradiation, the samples were placed on a copper disc with a potassium bromide cover and mounted in the sample chamber of the sample zone of the spectrometer, under ultrahigh-vacuum conditions. Samples were heated by successive power steps induced by a CO_2 laser with a maximum energy of 30 W. Every three analytical steps, blank measurements were made, to correct successive measurements.

Noble gases extracted from the sample were separated using a cold finger trap and one getter (ST101), operated at 2.2 A. Purified sample was introduced in the MAP 215-50 mass spectrometer. Isotope contents for masses ^{36}Ar, ^{37}Ar, ^{38}Ar, ^{39}Ar and ^{40}Ar were measured using a high-resolution electron multiplier, together with baseline measurements for every heating step.

The apparent ages obtained for every heating step take into account corrections for interference of isotopes generated during irradiation from K, Ca and Cl. The criterion for defining a 'plateau age' corresponds to three or more successive steps overlapping with an error at 2σ level and containing >50% of released ^{39}Ar (Fleck *et al*. 1977). The decay constant for ^{40}K used for calculations is that proposed by Steiger & Jäger (1977). The atmospheric ratio for $^{40}Ar/^{36}Ar$ is assumed to be 295.5.

Late Palaeozoic forearc section at Punta de Choros–Quebrada Chañaral

In this section, we show our new results on the stratigraphy, field relationship and petrography of Late Palaeozoic forearc units, aiming to separate different lithostructural associations. On the basis of these data, we recognize at least three tectonic components of the Late Palaeozoic forearc, which are described below: (1) the Punta de Choros Metamorphic Complex, which represents the basal accretionary prism; (2) the Chañaral Epimetamorphic Complex, which corresponds to a frontal accretionary prism; (3) the Llano de Chocolate Beds, interpreted as a forearc or retro-wedge basin deposits.

Local geology

Between 28°30′ and 29°30′S, the Carboniferous–Early Permian metamorphic rocks exposed along the coastline and western slope of the coastal ranges (Fig. 1b) comprise associations of micaschists, metabasites (greenschists and amphibolites) and low-grade metasediments (phyllites and metasandstones). Most micaschists and metabasites south of 29°S were assigned by Creixell *et al*. (2012) to the Punta de Choros Metamorphic Complex, whereas low-grade metasediments, which are dominantly exposed north of 29°S, were assigned to the Chañaral Epimetamorphic Complex by Welkner *et al*. (2006). The primary metamorphic mineralogy is partially overprinted by contact aureoles of 193–150 Ma Early to Late Jurassic plutons and mafic dyke swarms (193–150 Ma, Welkner *et al*. 2006; Creixell *et al*. 2012). Carboniferous to Permian sedimentary rocks are exposed directly east of the metamorphic rocks, and comprise an association of sandstones, conglomerates and shales, with interbedded fossiliferous limestones and tuffs. These are grouped as the Llano de Chocolate Beds, but most of these rocks were previously assigned to the Triassic Canto del Agua Formation (Moscoso 1979), with only a minor portion of the sequence recognized as Permian by the presence of brachiopod fossils (Welkner *et al*. 2006; Creixell *et al*. 2012). The Llano de Chocolate Beds are tectonically juxtaposed over Early Cretaceous volcanic rocks (Punta del Cobre Formation) by reverse fault systems (Fig. 1b).

Basal accretionary prism

This association is more widespread along the coastline and comprises fine- to medium-grained micaschists, with tens of metres thick intercalated slices of greenschists. Micaschists are the main constituent of this unit and they show a fabric defined by a flat-lying S_2 penetrative foliation (Fig. 2a), which transposes previous S_0 and S_1 fabrics. In some places an older S_1 foliation is preserved, transposed by a penetrative S_2 foliation (Fig. 2b). This last foliation also occurs parallel to flat fold axes affecting primary depositional contacts (S_0). Mineral lineation shows variable attitude but mostly tends to have an azimuth perpendicular to the foliation strike. NE–SW-striking, steep crenulation foliation is superimposed on S_2 in some outcrops, especially near Carrizalillo bay. At microscopic scale, the micaschists consist of a matrix of alternating granoblastic and lepidoblastic bands of minerals of greenschist metamorphic grade. The granoblastic bands are composed of recrystallized quartz and minor albite aggregates, and the lepidoblastic bands are composed of white mica, quartz and chlorite. White mica in the matrix is locally replaced by Fe–Al biotite close to Jurassic intrusive rocks. Magnetite, apatite, hercynite, chloritoid and zircon occur as accessory minerals. Pre-tectonic albite porphyroblasts show typical carbonaceous (graphite) inclusions, which have been well described in other localities of Late Palaeozoic micaschists (e.g. Godoy 1985; Hervé 1988). Garnet is scarce within these rocks. Greenschist slices have a dominant lithology of amphibole and chlorite schists, with a fabric defined by flat-lying S_2 foliation, similarly oriented to the micaschist fabric, but their mineral lineation is poorly developed. At microscopic scale, greenschists are mostly composed of pale green amphibole, accompanied by Mg-chlorite, epidote and quartz, magnetite (mostly as elongated aggregates) and minor albite (with apatite inclusions) and titanite. Retrogression is marked by the

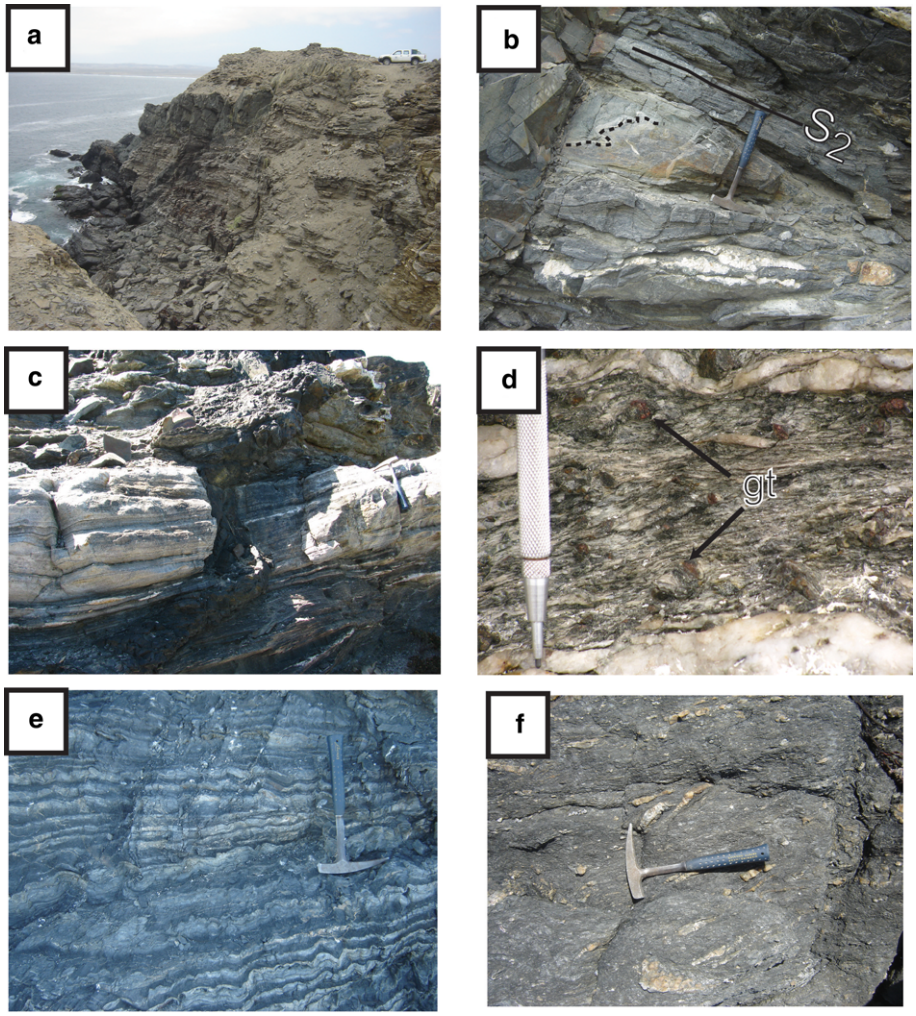

Fig. 2. Field features of basal and frontal accretionary prism; (**a**) flat-lying penetrative S_2 foliation in micaschist of basal accretionary prism; (**b**) penetrative S_2 foliation in metabasites, containing an older S_1 foliation (dashed line) in a competent bed of metasandstone; (**c**) light-coloured metachert intercalation parallel to main S_2 foliation, in a thick pile of metabasites from the basal accretionary prism; (**d**) macroscopic garnet porphyroblast in a coarse-grained micaschist at Isla Gaviota; (**e**) metaturbidites from the frontal accretionary prism exhibiting a steeply dipping crenulation cleavage that deflects original sedimentary contacts between metasandstones (light grey) and metapelites (dark grey); (**f**) mélange fabrics composed of light-coloured blocks of quartz pods in a matrix of foliated phyllite, frontal accretionary prism.

presence of Fe-rich chlorite veins and patches in the matrix. The most common porphyroblasts correspond to syntectonic albite and quartz. Calc-silicate rocks are characterized by coarse to medium grain size and a white colour (similar to granites) in outcrop. At microscopic scale, these rocks show a granoblastic texture consisting of zoned plagioclase, titanite, zoisite, rounded quartz, garnet with rotated inclusion trails and apatite, with a pervasive low-temperature assemblage of chlorite, magnetite, white mica and amphibole. Similar rocks further south (31°30′S) have been interpreted as retro-eclogites by García-Sansegundo *et al*. (2014).

North of Playa Apolillado and near Punta de Choros, two distinctive blocks of garnet-bearing schists, interpreted as tectonic slices, are dominated by foliated amphibolites (with or without macroscopic garnet porphyroblasts), some of them partially retrogressed to greenschists. At microscopic scale, the amphibolites are formed mostly by green calcic amphibole, accompanied by plagioclase, elongated titanite, epidote, rutile and opaque minerals with titanite rims. These rocks show intercalations of metachert (Fig. 2c), local pods of stretched garnet-bearing calc-silicate rocks and coarse-grained micaschists with centimetre-sized garnet porphyroblasts (Fig. 2d) of almandine-rich composition (Navarro 2013). Pre-tectonic staurolite and albite are also recognized in micaschists at Isla Gaviota. Some garnet porphyroblasts show asymmetric pressure shadows and rotated texture, indicative of syntectonic growth (Passchier & Trouw 2005). Retrogression to chlorite in these garnet crystals is recognized along borders and fractures. Geothermobarometric calculations along these tectonic slices performed by Navarro (2013) determined that garnet micaschists evolved following a prograde path, from 500°C/0.4 GPa to 530°C/0.42 GPa, whereas garnet amphibolites evolved along a counterclockwise metamorphic *P–T* path, from 700–800°C/0.8 GPa to 700°C/0.9 GPa, to reach final equilibrium conditions after isobaric cooling, in the stability field at 0.85–1.05 GPa and 500°C.

Frontal accretionary prism

This corresponds to an association of phyllites, slates and metasandstones, which are well exposed as stratified sequences at several localities along the western half of the study area (Fig. 1b). The main fabric of these rocks is a primary bedding, deformed by a millimetre- to centimetre-scale steep foliation defined by pressure-solution bands and cut by polydirectional quartz and carbonate vein systems. In some cases, foliation corresponds to a crenulation cleavage, spaced at tens of centimetres in rhythmic sequences of metasandstones and phyllites (Fig. 2e). Near Playa Apolillado, these rocks are tectonically juxtaposed with schists by a SW-vergent transpressive sinistral shear zone (Apolillado Shear Zone). Along this zone, metasandstones or phyllites contain a moderate to steep foliation that transposes original bedding and quartz pods. This foliation varies between planar foliation and axial plane foliation. In some cases, pencil lineation of aggregate minerals is present, as intersection between foliation and sedimentary bedding. Mineral lineation along foliation planes usually shows rakes between 30 and 65°. Mélange fabrics are also recognized in metaturbidites, and to a minor extent in micaschist (basal accretionary prism). These mélanges consist of blocks of quartz pods, phyllites or metabasites in a phyllite matrix (Fig. 2f). At the Quebrada Honda section, a complete gradational transition is observed from fine-grained phyllites to a sandstone and shale association, with an eastward decreasing degree of recrystallization. At microscopic scale, metasandstones from the frontal accretion series exhibit weak

foliation and are composed of quartz, feldspar and lithic grains, with serrate borders, with a fine-grained matrix of mostly silica, sericite and chlorite. Silica veins are common in these rocks. Phyllites are characterized by a fine-grained (0.01–0.04 mm) clastic texture of quartz + mica grains, obliterated by pervasive foliation, associated with pressure solution planes formed by opaque minerals and interlayered micas (sericite + chlorite). These planes show shear displacements, in some cases displacing quartz veins. Chevron crenulation locally folds the main foliation. Late biotite is common and is probably associated with contact metamorphism of Jurassic plutons and dykes.

Forearc basin

To the east, a thick sedimentary sequence consisting of conglomerates, sandstones, shales, limestones and volcanic rocks has been assigned by correlation to the Triassic Canto del Agua Formation (Moscoso 1979; Welkner *et al*. 2006). In spite of the lack of geochronological data for these rocks, Welkner *et al*. (2006) assigned a 300 m thick sequence of green marine sandstones and limestones to the Permian, based on brachiopod fauna, defined as the Llano de Chocolate Beds. This sequence was distinguished from the Canto del Agua Formation based on the stratigraphic age assigned to the latter, although the contact and separation of these two units was not clearly demonstrated. In this study, new U–Pb ages show that much of this sedimentary sequence, which has been considered as part of the Canto del Agua Formation and Triassic in age, is in fact of Late Carboniferous to Early Permian age (see discussion below) and thus is reinterpreted as part of the Llano de Chocolate Beds. In spite of this, the presence of *Choristoceras* sp., a Rethian ammonite, described by Godoy (1985) along the Sierra El Tofo (on the northern slope of Quebrada Chañaral), and early Jurassic *Spiriferina*, in the same area, indicates that part of the original Mesozoic Canto del Agua Formation has been deposited over the Permian sequence.

The field features of the sedimentary facies of this unit, defined in two stratigraphic sections measured at the Quebrada Honda and Quebrada Chañaral area (Fig. 1b), are shown in Figure 3. A noteworthy feature of the unit is the presence of conglomerates with large amounts of acidic volcanic clasts (Fig. 3a) and, more locally, with metamorphic clasts of schists and quartz fragments (Fig. 3b). A slight foliation in the matrix and stretched clasts are recognized at the base of the sedimentary pile. A striking feature of this sequence is the transitional contact with overlying metasediments assigned to the frontal accretion series (mostly metaturbidites). An angular unconformity between the two units has been reported, however, from outcrops in the shoreline near Huasco (28°S, Welkner *et al*. 2006). The transitional change from frontally accreted metasediments to the sedimentary pile is well exposed along the Quebrada Honda section. At this locality, phyllites and metasandstones with steeply dipping structures grade into deformed sandstones and shales and then to foliated coarse conglomerates.

The prograde character of the identified facies associations suggests that the deposit corresponds to a deltaic system, with the typical architectural elements of this environment, such as a delta plain and its distributary channels (F1, F2), delta front (F3, F4) and prodelta (F5, F6). Particular features are the inner shelf bar (F7) and the distributary channels within the delta front and prodelta (F8) facies, suggesting a tide-dominated delta. The volcanic activity-related facies (F9–F11) are interpreted as the result of both *in situ* and distant volcanism of acidic composition.

In terms of its vertical evolution, the depositional sequence of the Llano de Chocolate Beds starts with the pyroclastic fall deposits emplaced near the shelf, as suggested by the interbedded grainstone of F9. Later, the prodelta facies developed and distributary channels reached the open basin probably in periods of intense fluvial discharge (F10). The origin of the regression character of the sequence is unclear but it later evolves to a well-developed prograde system as the base level of the basin migrates landward and then is stabilized at facies F4. A high normal regression period is represented by the transition from prodelta (F6) to delta front (F3) facies, indicating a sediment supply not fully accommodated in the basin. A forced regression is represented by the volcanic and debris flow facies (F11 and F9) that supplied material from areas of positive topographic relief, which were probably elevated by tectonic forces. This regression ends with an erosive process recorded in the sedimentary sequence at the top of facies F9 (Fig. 4). After a new landward displacement of the base level a new low normal regression period is recorded in the prodelta and volcanic facies (F5, F6 and F14) overlain by delta plain facies (F1 and F2) with a maximum regression surface at the top of this sequence. Finally, a transgression period is recorded by the delta front facies (F3) at the top of the entire section (Fig. 4).

Geochronological constraints

Detrital zircon ages

U–Pb ages from detrital zircons of the Llano del Chocolate Beds were obtained from outcrops at Quebrada Honda (CPV-12-82), from a section along Quebrada Chañaral (CPV-12-126) and from a section east of Quebrada Algarrobo (CPV-12-124).

At Quebrada Honda, one sample (CPV-12-82) corresponds to a sandstone located directly below a coarse-grained conglomerate level. Below the sandstone level, a thick pile of shales, sandstones and phyllites is recognized. In this sample, 86 grains were measured, bracketing the age interval between 269 and 2581 Ma (youngest and older grains, respectively; Fig. 5a). In the complete population of zircon ages, the largest group is of Late Carboniferous age (*c*. 313 Ma), with a second population of Cambrian age (514 Ma) and a Mesoproterozoic (Ectasian) peak near 1220 Ma. Considering the younger ages ($n = 30$) in more detail, a young Early Permian age population is clearly distinguished (292.1 ± 5.6 Ma), with a larger population at 313.9 ± 1.8 Ma and secondary peaks at 342.1 ± 8.2, 360.2 ± 6.9 and 382.0 ± 5.9 Ma.

A sandstone sample (CPV-12-124) from the Quebrada Chañaral section yields detrital zircon U–Pb ages in the range between 267 and 373 Ma (Fig. 5b), with six age populations determined through ISOPLOT (Ludwig 2003) unmixing ages ($n = 97$) grouped at 272.9 ± 5.8 Ma (maximum depositional age) and 286.6 ± 4.1, 294.8.5 ± 3.5, 302.9 ± 1.3, 312.4 ± 3.1 and 374 ± 20 Ma. It should be noted that three younger ages were omitted from the analysis because of lack of statistical support and uncertain stratigraphic consistency.

Along the Quebrada Chañaral, we obtained U–Pb zircon ages from a litharenite (CPV-12-126). The youngest age population represents a maximal depositional age of 291.7 ± 2.8 Ma (Fig. 5c), with older populations grouped at 301.3 ± 1.7, 316.2 ± 2.8, 343.8 ± 16.0, 391.5 ± 7.6 and 577.3 ± 8.3 Ma, estimated through ISOPLOT unmixing ages ($n = 90$). Seven younger ages were excluded from the interpretation because they have no statistical support and are not consistent with the stratigraphic location of the sample.

Zircon U–Pb crystallization ages

We analysed three samples of volcanic rocks (dacite, rhyolite and tuff) collected along the Quebrada Chañaral section. These rocks are interbedded with the sedimentary sequence of the Llano del Chocolate Beds (Fig. 4). For the rhyolite sample CPV-12-105, a well-constrained (MSWD = 0.031) concordia U–Pb age of 318.8 ± 2.5 Ma was obtained, from a single population of zircon crystals (Fig. 6a). The dacite sample (CPV-12-12) is from a dome intercalated in the middle part of the sequence. In this sample, we obtained a U–Pb concordia age in zircons of 303.8 ± 2.7 Ma

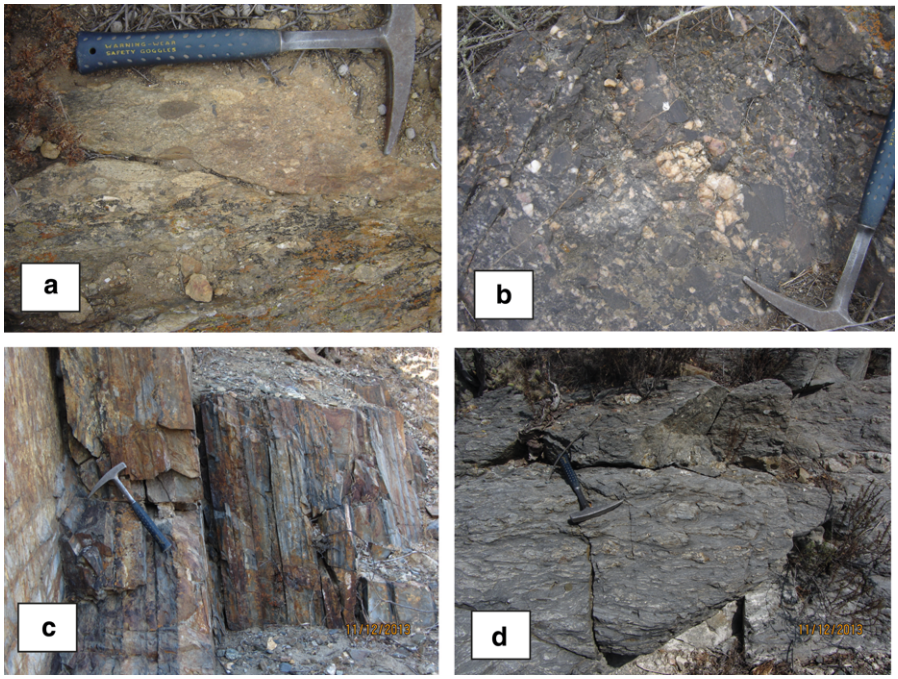

Fig. 3. (**a**, **b**) Field features of the Llano del Chocolate Beds: (**a**) foliated conglomerate with rhyolitic volcanic clasts at the base of the sequence; (**b**) coarse breccia-like deposits, consisting of dominant quartz clasts of metamorphic origin, in a fine-grained sandstone matrix. (**c**, **d**) Field features of the Chañaral Epimetamorphic Complex: (**c**) decimetre-scale intercalation of slightly recrystallized metasandstones and metalutites near the contact with the Llano de Chocolate Beds; (**d**) well-foliated mélange facies with protomylonitic fabric.

(MSWD = 0.52, Fig. 6b), which represents the crystallization age for the dacite dome. The tuff sample (CPV-12-127) has four age populations ($n = 98$) of 291.4 ± 0.8, 299.9 ± 0.5, 306.8 ± 0.7 and 322.8 ± 1.8 Ma (Fig. 6c), where the youngest age of 291.4 ± 0.8 Ma is considered the maximum depositional age.

Ar–Ar ages of metamorphic rocks

Four new $^{40}Ar/^{39}Ar$ determinations in white mica and biotite from schists from the Punta de Choros Metamorphic Complex are described here. Additionally, three $^{40}Ar/^{39}Ar$ ages (samples CI-165, CI-09 and CI-137) previously published by Creixell *et al.* (2012) for schists from the Punta de Choros Metamorphic Complex have been included here for reinterpretation in the light of the new results.

The four new $^{40}Ar/^{39}Ar$ ages are interpreted in terms of a perturbation from the original age, probably caused by Ar loss or diffusion by a reheating event, such as the intrusion of the Early Jurassic La Vaca granodiorite or the redistribution of Ar by slow cooling or secondary deformation events, as these are detected at outcrop and thin-section scale.

A sample of fine-grained micaschist from Choros Island (CI-148) is characterized by the presence of syntectonic biotite porphyroblasts and a matrix with abundant folded white mica, quartz, and white mica pods and bands, pre-tectonic garnet and rotated albite crystals. The obtained $^{40}Ar/^{39}Ar$ plateau age of 279.5 ± 2.2 Ma includes 51% of the released ^{39}Ar and can be interpreted only as a minimum age for the main metamorphic event. The step-heating spectra for this sample show younger apparent ages for the first three steps (A–C) reflecting the effect of gas liberation from inclusions or partially neoformed or recrystallized white mica (Fig. 7a), suggesting that an undetermined proportion of Ar loss occurred after the time of primary closure of muscovite (375 ± 25°C, Hunziker *et al.* 1992). It is difficult to determine with certainty the original composition of Ar fluids, owing to the low $^{36}Ar/^{40}Ar$ ratios and strong clustering of measurements in the inverse isochron diagram (Fig. 7b).

Discordant results have been obtained in the geochronological record from biotite and muscovite from sample CI-164, despite both minerals being overgrowths along foliation planes, without apparent younger or recrystallized grain populations. Muscovite from this sample yields a plateau age of 229.7 ± 0.3 Ma (Fig. 7c) including 87% of the released ^{39}Ar. Low-temperature steps reveal a small amount of Ar loss. As in the previous sample, the initial composition of Ar fluids is poorly contrasted, owing to strong clustering of measurements, with $^{36}Ar/^{40}Ar$ ratio close to zero (Fig. 7d). The biotite sample show a similar step-heating pattern and also clustering in the inverse isochron diagram (Fig. 7f), but the obtained plateau age is younger, at 206.3 ± 0.4 Ma (Fig. 7e). In spite of the fact that well-determined plateau ages could indicate the presence of a young (Triassic) deformation event in the Punta de Choros Metamorphic Complex, uncertainty in the composition of Ar indicates that these ages need to be interpreted with caution.

The step-heating pattern of muscovite sample CI-135 yields a plateau age of 190.2 ± 0.4 Ma (Fig. 7g). The first three degassing steps reveal a small amount of Ar loss or the presence of inclusions in the muscovite, whereas the slightly older steps D and E are probably affected by excess Ar (relict Ar from primary metamorphic composition) or ^{39}Ar loss by recoil during irradiation (Fig. 7h). Because the age of this sample is concordant with the age of La Vaca granodiorite, we suggest a major resetting of the age by this young event.

Amphibole analyses have been obtained from a medium-grained garnet amphibolite (sample CI-165) from a tectonic slice of garnet-bearing schists, as described above. A plateau age of 320.5 ± 1.5 Ma, comprising 78% released ^{39}Ar, is obtained (Fig. 8a), but a $^{40}Ar/^{36}Ar$ ratio of 344 ± 10 in the inverse isochron diagram suggests an excess Ar component (Fig. 8b). The corrected age for the sample is 319.0 ± 1.4 Ma. However, the composition of the trapped Ar of the sample is not well constrained, because of the small ^{36}Ar and/or high radiogenic ^{40}Ar component, giving large uncertainties in the inverse isochron diagram (MSWD = 8.9). Considering a closure temperature around 450 ± 50°C for the Ar system in amphibole (Baldwin *et al.* 1990), this age around 319 Ma is interpreted as being close to the time of metamorphism after peak conditions and isobaric cooling described for this amphibolite (Navarro 2013).

A medium-grained garnet micaschist (metapelite) exposed close to the amphibolite sample CI-165 was analysed for muscovite (sample CI-09). In this sample, the degassing pattern does not form a plateau, but is a staircase pattern, with higher apparent ages in the low-temperature steps, and may be interpreted as a consequence of Ar redistribution, with a large excess ^{40}Ar component in low-temperature steps, probably associated with diffusion processes during progressive metamorphism (Fig. 8c). This is also observed in

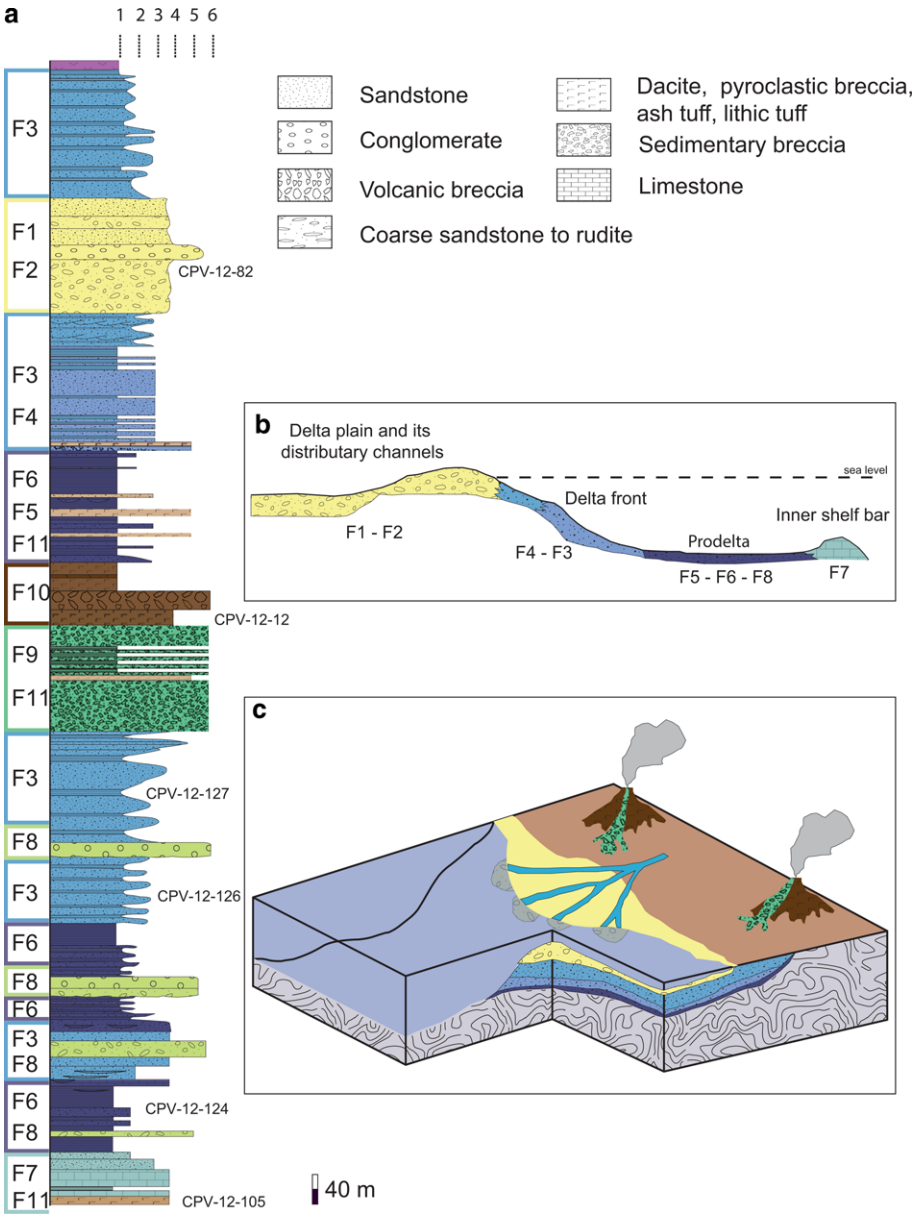

Fig. 4. Llanos de Chocolate Beds stratigraphy: schematic stratigraphic section of the Llano del Chocolate Beds, including sedimentary facies and the interpreted environment in (**b**) 2D view and (**c**) 3D view. Clast or fragment sizes in the section are: 1, <0.062 mm; 2, 0.062–0.25 mm; 3, 0.25–0.5 mm; 4, 0.5–2 mm; 5, 2–64 mm; 6, 64–256 mm.

the $^{36}Ar/^{40}Ar$ intercept at 1300 ± 11 in the inverse isochron diagram (Fig. 8d). The calculated age in the inverse isochron is 260.7 ± 0.6 Ma, considering all of the steps except B, C and E.

Sample CI-137 is another medium-grained garnet micaschist (metapelite) with penetrative foliation, from the tectonic slice where garnet amphibolite is recognized. In this sample, a plateau age of 263.0 ± 5.0 Ma for muscovite grains is defined in the intermediate steps, comprising 61.4% of the released ^{39}Ar (Fig. 8e). However, older ages at low-temperature steps and younger ones at high-temperature steps suggest that significant redistribution of Ar isotopes occurred in this sample, as a probable effect of ^{39}Ar recoil during irradiation. Because the integrated age is similar to the plateau age obtained in this sample the latter is considered as the main age for this sample. This age must be interpreted with caution.

Discussion

Tectonic significance of metamorphic P–T–t *paths of the Punta de Choros Metamorphic Complex*

The new geochronological constraints on the age of crystallization of the Punta de Choros Metamorphic Complex define a broad range of evolution of this complex between 319 and 263 Ma. Because metamorphic conditions of crystallization are largely contrasting along the complex, we can identify an old metamorphic event, dated at 319 Ma, associated with a tectonic slice of garnet amphibolites and micaschists. The counterclockwise *P–T* trajectory of the garnet amphibolite sample determined by Navarro (2013) indicates that after deep burial of the material along the subduction channel to peak conditions at 700°C/0.95 GPa, the block was cooled isobarically to final equilibrium conditions at 500°C/0.85 GPa (Fig. 9). In contrast to these crystallization conditions, a sample of garnet micaschist from another tectonic slice recorded moderate temperatures and pressures at peak conditions (530°C/0.42 GPa; Fig. 9), suggesting that exhumation of tectonic slices occurred from variable depths in the accretionary prism. Assuming a closure temperature around 450 ± 50°C for amphibole (Baldwin *et al.* 1990), the $^{40}Ar/^{39}Ar$ age of 319 Ma in the amphibolite is a minimum age for this amphibolite-facies metamorphism after peak conditions. It is worth noting that garnet amphibolite is scarce in the metabasite slices, and that it represents a high-*P*/high-*T* relict facies surrounded by late retrograde greenschist-facies metabasites, in a similar fashion to retro-eclogite–amphibolite relict blocks have been recorded in the basement at 31°30′S (García-Sansegundo *et al.* 2014) and much further south (e.g. Kato *et al*. 2008). The younger

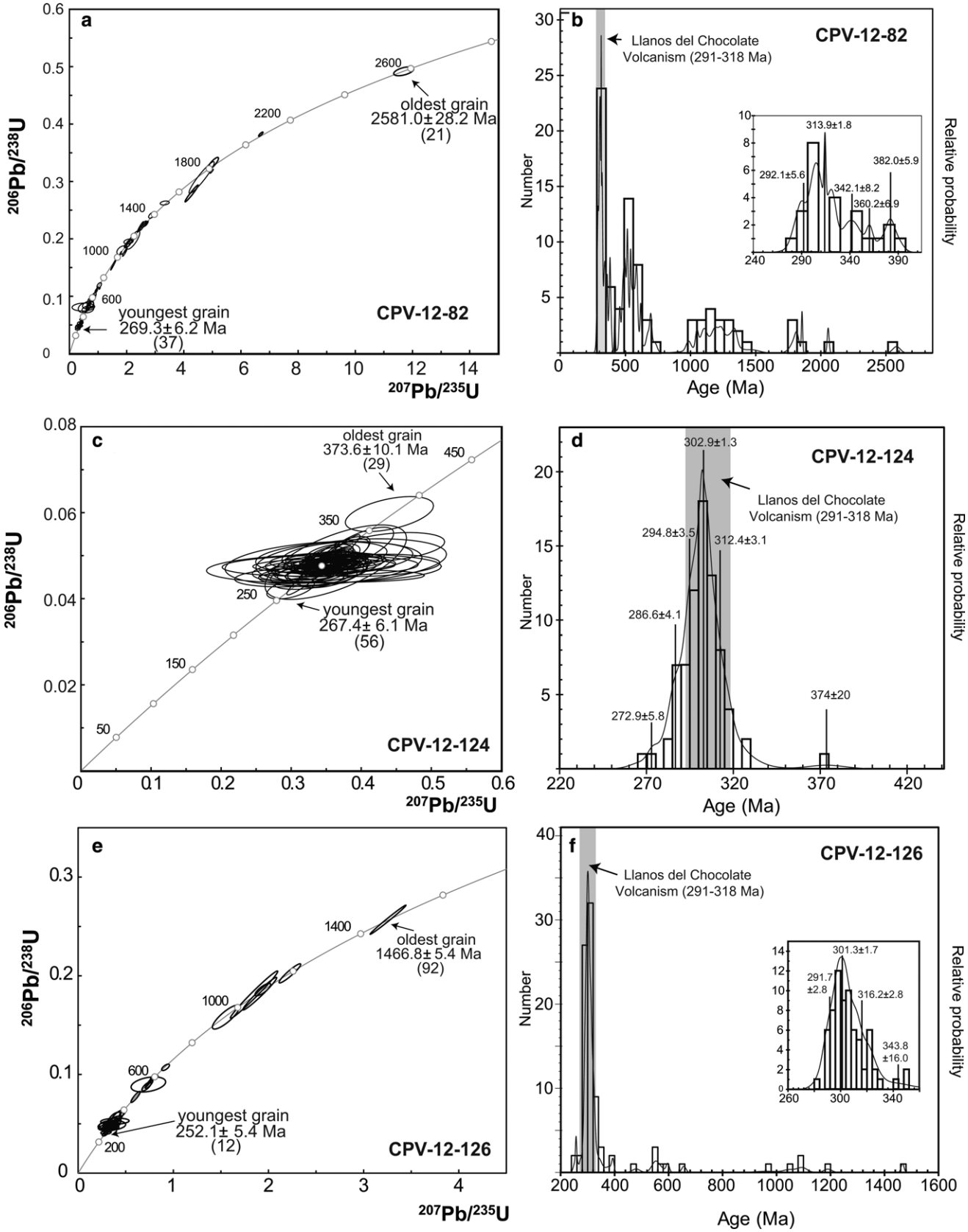

Fig. 5. (**a**, **c**, **e**) Concordia diagrams from detrital zircon ages from Llano de Chocolate Beds. (**a**) Sample CPV-12-82 is a sandstone from Quebrada Honda section; (**b**) sample CPV-12-124 is a sandstone from Quebrada Chañaral; (**c**) sandstone sample from Quebrada Chañaral. (**b**, **d**, **f**) Probability density plots for the same samples.

$^{40}Ar/^{39}Ar$ age around 280 Ma determined in micaschists in the Punta de Choros Metamorphic Complex could be related to the continuation of basal accretion until Early Permian times, but 260–263 Ma ages determined in samples CI-09 and CI-137 are considered as minimum (cooling?) ages, probably related to fluid circulation in the wedge, as metamorphic conditions in the block containing these micaschists reached a high temperature, around 700–500°C (Navarro 2013).

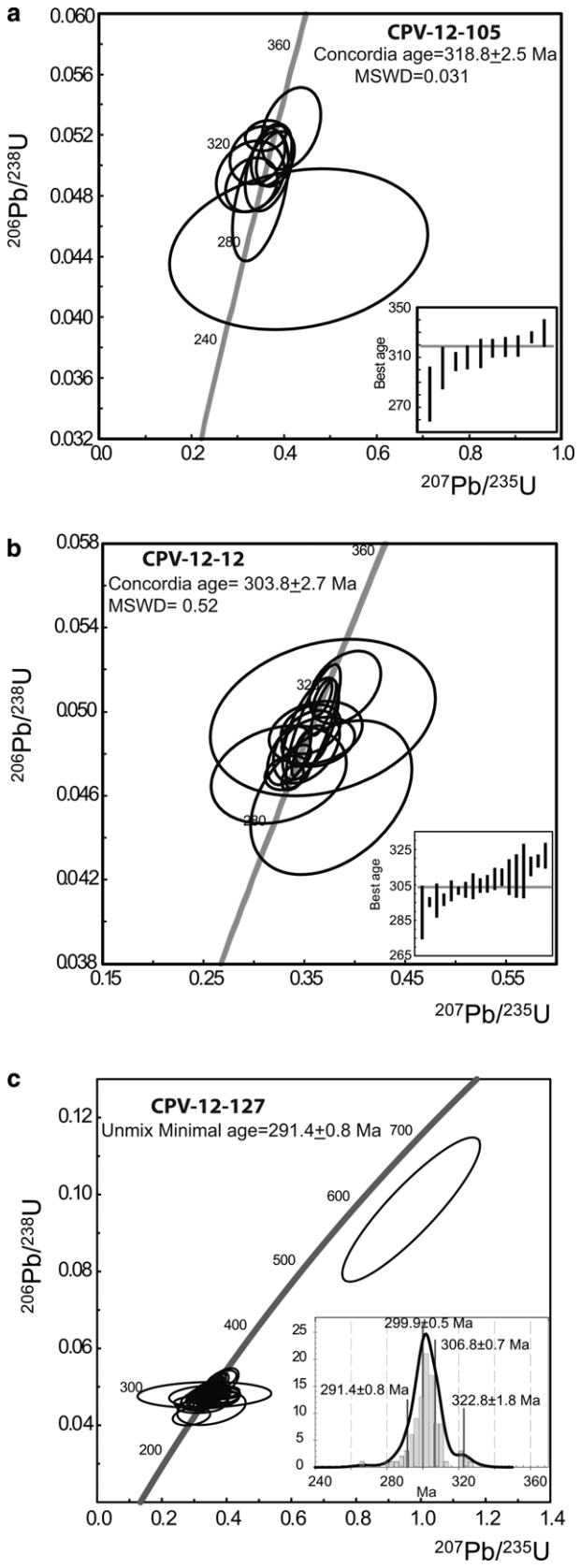

Fig. 6. Concordia diagrams from igneous zircon ages from volcanic rocks of the Quebrada Chañaral section, Llano de Chocolate Beds. (**a**) Rhyolite sample CPV-12-105; (**b**) dacite dome sample CPV-12-12; (**c**) tuff sample CPV-12-127.

The peak and final temperature (700–500°C) recorded in the tectonic slice of garnet amphibolites reflects a high thermal gradient, which is unexpected for a forearc area (Peacock 1996). According to the literature, these high-pressure slices are a persistent feature of Late Palaeozoic accretionary prisms exposed along the Chilean coastal margin. Hyppolito *et al*. (2014) described a large coherent block ('Infiernillo unit') recognized in the coastal metamorphic complex around 34°S, characterized by anticlockwise *P–T–t* trajectories, reaching amphibolite-facies metamorphism at peak conditions (Fig. 9). In the same fashion, remnants of amphibolite-facies blocks are preserved in generalized greenschist-facies metamorphic complexes at the Choapa and Bahia Mansa metamorphic complexes (Fig. 9; Kato *et al*. 2008; Willner *et al*. 2012). Possible explanations for a high thermal gradient in the forearc may be the subduction of an active and hot ridge from the oceanic plate or a high thermal gradient that occurred during the onset or renewal of the subduction system during Mississippian times. The first possibility is discarded for this area, because magmas produced in this condition lack typical calcalkaline signatures, but show ocean island basalt or adakitic signatures, which are not recorded in Late Palaeozoic granitoids along the margin (Mpodozis & Kay 1992). The second possibility for the high thermal gradient will be discussed below. A third model has been advanced by Godoy & Navarro (2014), who linked this forearc high thermal gradient to extended partial melting of the continental crust during the Permian, associated with the construction and presence of the magmatic arc.

Sources of detrital zircon ages in Llano de Chocolate Beds and implications in crustal exhumation history

According to zircon age populations that record the U–Pb ages presented here for sedimentary rocks, the possible sources for detrital input to the Llano de Chocolate Beds are very variable from north (Quebrada Honda) to south (Quebrada Chañaral). In general terms, the more persistent age peak (Late Carboniferous–Early Permian) in the detrital zircon patterns from the two analysed sandstones from Quebrada Chañaral coincides with the period of volcanism of this unit (291–318 Ma) recorded by the U–Pb crystallization ages. Indeed, the statistical distribution of zircon ages in the two sandstones is typical for volcanic areas (e.g. Cawood *et al*. 2012). For example, the zircon age pattern for sample CPV-12-124 has 86% of ages in the range 318–291 Ma. The facies distribution in the stratigraphic column also suggests that volcanic centres were proximal to sediments, as volcanic rocks are mostly domes or rhyolite bodies. Given that these volcanic sources were close, it is very likely that the maximum depositional ages are close to the actual time of deposition of the sediments. These observations in conjunction with petrographic features, such as abundance of rhyolitic and monomineralic quartz clasts in sandstones and conglomerates, suggest that zircon age peaks are related to reworking of acidic volcanic products erupted coeval with the main sedimentation of the Llano de Chocolate Beds, especially in the Quebrada Chañaral section. In contrast, the zircon age pattern obtained for the sample from Quebrada Honda (CPV-12-88) has only 21% of the ages falling within the range for the volcanic rocks. This decrease in these ages for this sample may be linked to the deposition of the sediments in this section in a position far from volcanic centres, in comparison with the south.

Apart from possible volcanic sources in the detrital record, other possible sources, in great part masked by the volcanism, may be deduced for the Llano de Chocolate Beds. Indeed, it is possible to identify an important source of metamorphic rocks in coarse-grained sedimentary rocks, especially at the bottom of the sequence (Fig. 3b). In the sample from Quebrada Honda (CPV-12-88) zircon age peaks older than 318 Ma are identified, especially a zircon age population around 334 Ma and a Pampean (*c*. 500 Ma) population. The former age peak is identical to the 334 ± 6 Ma reported by Navarro (2013) for a micaschist from the Punta de Choros Metamorphic Complex. These age similarities, in addition to the

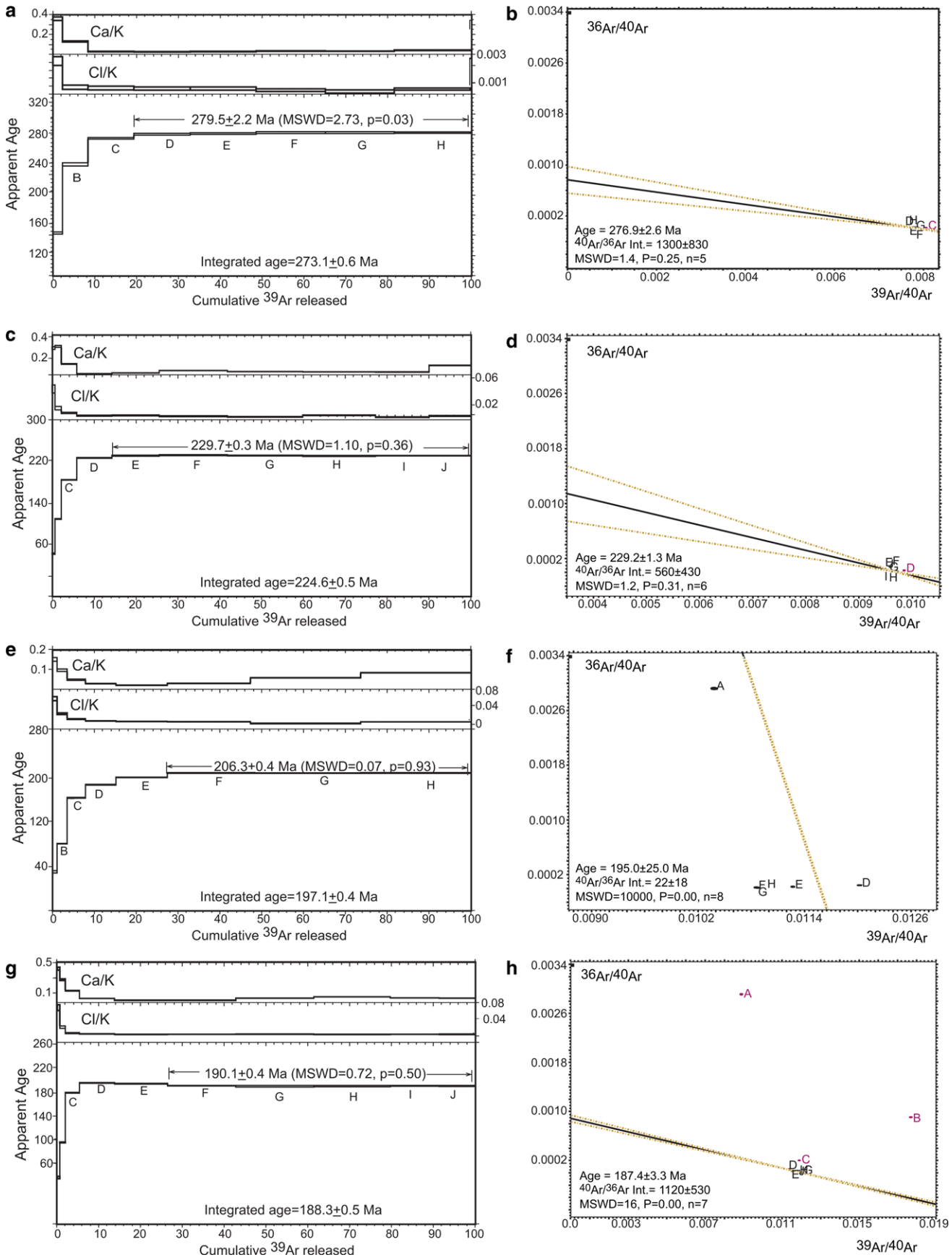

Fig. 7. Step heating diagrams and inverse isochrons for $^{40}Ar/^{39}Ar$ ages from micaschists of the Punta de Choros Metamorphic Complex. (**a**) Step-heating degassing pattern for muscovite from the micaschist sample CI-148; (**b**) inverse isochron; (**c**) degassing pattern from step-heating for muscovite sample CI-164; (**d**) inverse isochron; (**e**) degassing pattern from step-heating for biotite sample CI-164; (**f**) inverse isochron; (**g**) degassing pattern from step-heating for muscovite sample CI-135; (**h**) inverse isochron.

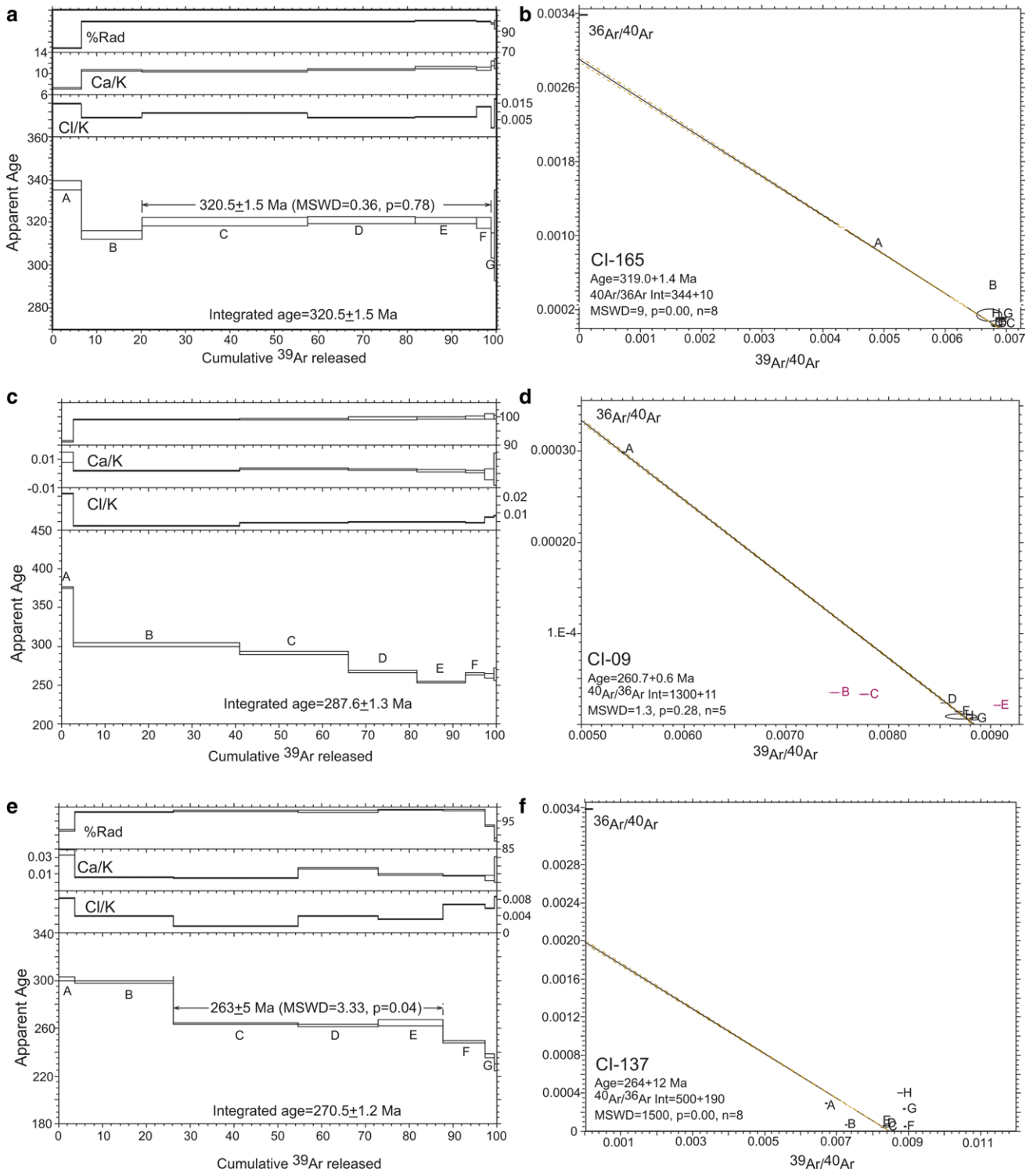

Fig. 8. Step heating diagrams and inverse isochrons for $^{40}Ar/^{39}Ar$ ages from micaschists of the Punta de Choros Metamorphic Complex.

observed abundance of metamorphic clasts at the base of the Llano de Chocolate Beds, suggest that the Punta de Choros Metamorphic Complex was an important detrital source in the forearc basin. However, we cannot discard that other sources for Devonian zircons, such as the Achala Batholith (Dahlquist *et al*. 2013) exposed at Sierras Pampeanas, were involved.

Because the older $^{40}Ar/^{39}Ar$ ages of metamorphism overlap with the age of the Llano de Chocolate Beds, we propose that sedimentation, volcanism, basal accretion and exhumation of metamorphic slices occurred contemporaneously along this forearc section. This interpretation cannot exclude that other sources of similar age, exposed far to the east, such as large Carboniferous plutonic complexes and volcanic rocks (Salazar *et al*. 2013; Maksaev *et al*. 2014) could be involved as clastic sources to the forearc. However, tectonic studies in the area suggest that exhumation of Carboniferous to Permian plutonic complexes along the high Andes took place around Early Triassic times, during development of the extensional San Félix basin (Salazar *et al*. 2013).

Geodynamics of the forearc and the origin of volcanism in the forearc

The geochronological data presented here point to a potential contemporaneity of metamorphic and sedimentary units along a

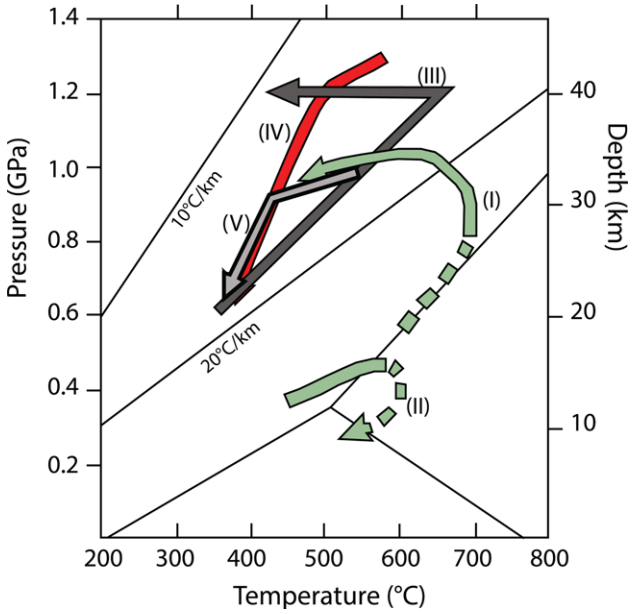

Fig. 9. Pressure–temperature diagram showing the metamorphic trajectories for the components of Late Palaeozoic accretionary complexes of north to south Chile. (I) garnet amphibolite of the Punta de Choros Metamorphic Complex after Navarro (2013); (II) garnet metapelite of the Punta de Choros Metamorphic Complex after Navarro (2013); (III) garnet amphibolite from the Bahia Mansa Metamorphic Complex (Kato *et al.* 2008); (IV) garnet metapelite and (V) garnet amphibolite from the Infiernillo Unit near 34°S (Hyppolito *et al.* 2014).

Late Palaeozoic forearc section. This is consistent with field data that suggest transitional changes from frontally accreted metaturbidites and sedimentary strata of the Llano de Chocolate Beds, and also with the transition from epizone to anchizone metamorphic grade in these units determined from illite crystallinity estimations (Alarcón *et al.* 2015). Thus, the outer boundary of the forearc basin represented by the Llano de Chocolate Beds could have been very close to the deformation front of the accretionary wedge.

A similar architecture of forearc basins in the proto-Andean margin has been proposed at 31°30′S (García-Sansegundo *et al.* 2014), where a highly subsident retro-wedge basin (Arrayán Formation) trapped most of the sediments, generating a starved trench during the Early Carboniferous. As deformation expanded landward during the Late Carboniferous to Early Permian, the previous forearc basin and accretionary prism (Choapa Metamorphic Complex) emerged, supplying sediments to the trench and to a new forearc basin (Huentelauquén Formation), which developed above and closely contemporaneous with the accretionary prism (Willner *et al.* 2012). Subsequent contractional phases brought in contact the undeformed forearc basin sediments and the metamorphic sedimentary and volcanic rocks representing the prism and obducted oceanic crust (Rebolledo & Charrier 1994). Although there are similarities in the deformational styles and lithologies between the Choapa and Punta de Choros metamorphic complexes and related sedimentary sequences, in this study area at 29°S, low-angle thrusts have not been recognized. A current example of a forearc basin closely related to the deformation front of the accretionary prism is the Aceh basin in the north Sumatra region (Mosher *et al.* 2008). There, the seaward flank of the forearc basin grades into a series of minor basins, located at the deformation zone, fed by topographic highs developed in response to landward-vergent thrusts that exhume part of the deformed accretionary prism. No major structures, putting in contact the deformed and undeformed rocks, are reported in this area. A similar situation could have existed during the development of the Llanos de Chocolate basin.

Another striking feature of this segment of the proto-Andean margin is the presence of Late Carboniferous to Early Permian acidic volcanism at the forearc. Few Palaeozoic volcanic units have been documented for the coastal region between 27° and 33° S, but, on the other hand, well-known Late Carboniferous to Early Permian plutonic complexes and minor volcanic rocks crop out extensively along the high Andes between 27° and 31°S, and along the coastal ranges south of 33°S. Other, but indirect evidence of Late Palaeozoic magmatic rocks in the coastal ranges between 29° and 33°S is the existence of scarce granitic xenoliths of Carboniferous age contained in Mesozoic mafic dykes at Punta Claditas (32°S, Berg & Charrier 1987). Although the igneous rocks in the study area are scarce, locally they represent a significant portion of the Palaeozoic forearc as detrital material and therefore are a major contribution to the forearc sedimentary basin. The age of the volcanic rocks recognized in the Llano de Chocolate beds is broadly concordant with two main episodes of arc plutonism at the same latitude, occurred at 324–316 and 295–284 Ma (Salazar *et al.* 2013; Hervé *et al.* 2014; Maksaev *et al.* 2014). These rocks are exposed 80 km to the east, in the high Andes cordillera, but we cannot discard that their original position could have been modified by Mesozoic extension (Mpodozis & Ramos 1989). Given the proximity of the volcanism to the accretionary prism and the evidence of significant input of volcanic material to the forearc basin, it is likely that this magmatic activity developed in the forearc region rather than within the arc domain.

The origin for the presence of this volcanism along the forearc section can be explained by the high thermal gradient recorded in garnet amphibolite. At the peak conditions reached by these rocks along the subduction channel (700°C/0.9 GPa, Navarro 2013), pelitic rocks, such as those intercalated with the amphibolites, could melt by dehydration-melting with breakdown of muscovite, generating a granitic melt with at least 4% dissolved water content (e.g. Miller *et al.* 2003). These melt compositions, even at low production rate, could easily explain the presence of rhyolites and dacites along the forearc (Fig. 10). To the south, this hypothesis could explain the presence of Late Carboniferous granitic xenoliths along the coastal area in dykes intruding the Choapa Metamorphic complex, and also could account for the presence of Carboniferous and Early Permian granite and rhyolite pebbles in the Huentelauquén Formation. The origin of the anomalous high thermal gradient in these rocks and therefore along the subduction zone cannot be resolved with our data, but we can relate it to the conditions at the onset or renewal of subduction at the continental margin, as the thermal state of subduction zones during onset typically allows the accretionary prism to reach high to moderate thermal gradients (Perchuk *et al.* 1999). Then, continuing plate convergence progressively cools the subducted slab until the 'normal' steady state of the subduction zone is reached, also facilitating isobaric cooling recognized along some counterclockwise metamorphic *P–T* paths, as in the Punta de Choros Metamorphic Complex (Navarro 2013). A similar hypothesis was proposed by Hyppolito *et al.* (2014) for the 'Infiernillo Unit' near 34°S. Also, Kato *et al.* (2008), on the other hand, documented the presence of eclogites and garnet amphibolites as exotic blocks in the blueschist zone of the accretionary complex at Los Pabilos (42°S), and those researchers interpreted these rocks as the relicts of the onset of subduction during the Late Devonian at that latitude. The hypothesis for the presence of garnet amphibolite blocks as relicts of subduction initiation is consistent with some field observation of migmatitization in some garnet micaschists that occur close to these garnet amphibolites. As the amphibole $^{40}Ar/^{39}Ar$ age in garnet amphibolite is considered as a minimum age for the metamorphism, we could suggest that onset of subduction occurred earlier, consistent with the presence of 324 Ma diorites as the first

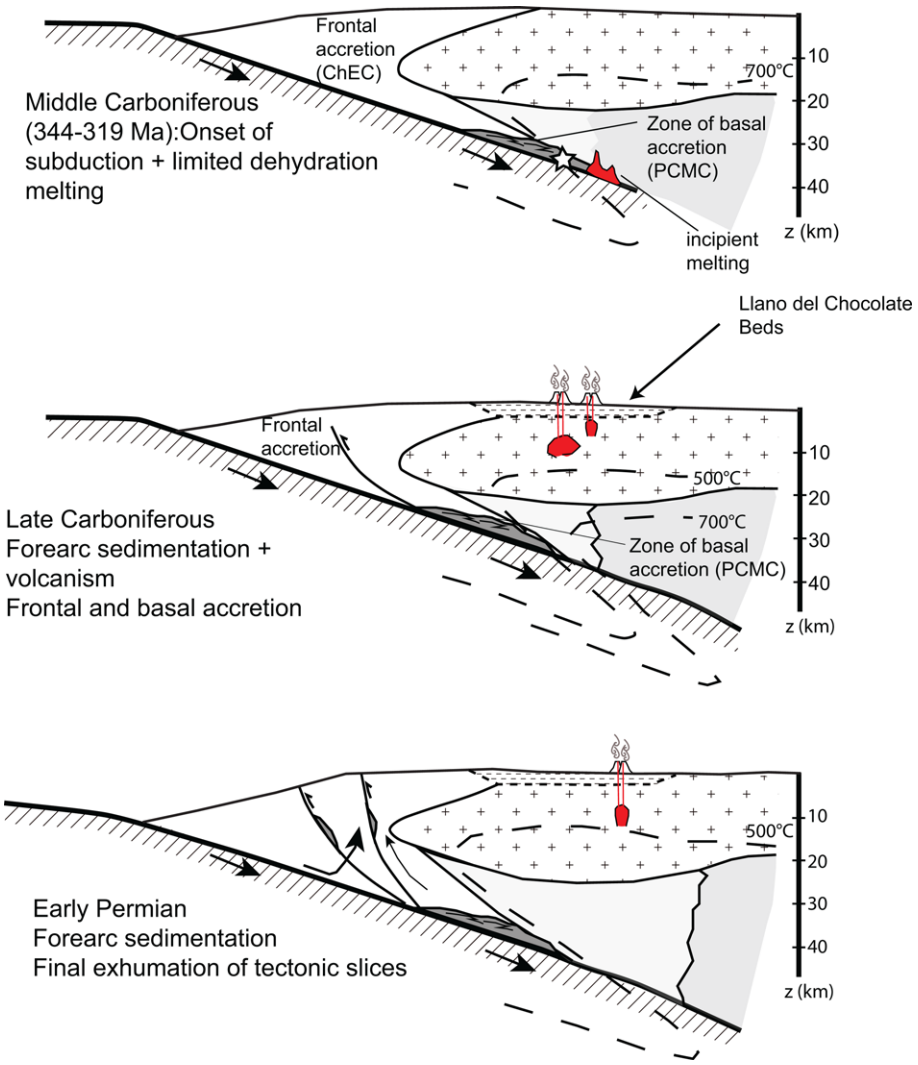

Fig. 10. Evolutionary sketch showing the main geodynamics features of the Late Palaeozoic forearc exposed along the coastal ranges between 28°30′ and 29°30′ S. ChEC, Chañaral Epimetamorphic Complex; PCMC, Punta de Choros Metamorphic Complex.

episode of arc magmatism recognized along the high Andes at this latitude (Fig. 10; Salazar *et al*. 2013).

Concluding remarks

A complete forearc section of the Late Palaeozoic continental margin of Gondwana is exposed at 28°00′–29°30′S and has been described in this contribution as formed by three subunits, the Punta de Choros Metamorphic Complex, representative of basal accretion series, the Chañaral Epimetamorphic Complex (frontal accretion series) and the Llano de Chocolate Beds, which represent the sediments that filled a forearc basin. The accretionary prism was developed through frontal and basal accretion, in addition to exhumation of at least two tectonic slices of garnet-bearing rocks, previously buried at variable depths. Field data indicate that sedimentation in the forearc basin took place contemporaneously with the development of frontal accretion in the accretionary prism during Late Carboniferous to Early Permian times. The older event recorded by our data at 319 Ma in the accretionary prism corresponds to the metamorphism at amphibolite facies of a tectonic slice containing garnet amphibolites and garnet micaschist to gneiss. These rocks record peak metamorphic conditions at 700°C/0.9 GPa. We suggest that these metamorphic conditions were reached in the subduction channel during the onset of subduction in the Late Carboniferous. This is consistent with regional data and the record of ages in the magmatic arc rocks exposed 80 km to the east.

The Llano de Chocolate Beds were deposited during continued small-volume acidic volcanism, in a delta-dominated sedimentation regime. The source for the sediments is mostly volcanic in the Quebrada Chañaral section, whereas in the Quebrada Honda section the sources are volcanic and from the Punta de Choros Metamorphic Complex, the latter especially for the bottom beds, as suggested by U–Pb and Ar–Ar age data. This indicates that part of the metamorphic complex was exhumed during the subduction and accretion process.

Our model suggests that basal accretion series, during the onset of subduction, were metamorphosed at a high thermal gradient, which was sufficient to melt small volumes of subducted material. These melts ascended and were emplaced as domes and tuffs in the Llano de Chocolate Beds. The final evolutionary stage for the forearc occurred in Late Permian times, when massive fluid infiltration and exhumation of the accretionary wedge took place, before partial thermal resetting of these rocks by Mesozoic intrusions.

Acknowledgements and Funding

This research was funded by a Fondecyt Grant (1120715) to V.O., C.C. and P.V., and Plan Nacional de Geología from SERNAGEOMIN. Additional funds were obtained from a Fondecyt Grant (1095099) for E.G. and J.N. The authors thank M. Yañez for his assistance in $^{40}Ar/^{39}Ar$ geochronology, C. Barra for mineral separation and R. Tello for his assistance in the field.

Scientific editing by Anna Bird

References

Agard, P., Yamato, P., Jolivet, L. & Burov, E. 2009. Exhumation of oceanic blueschists and eclogites in subduction zones: Timing and mechanisms. *Earth-Science Reviews*, **92**, 53–79.

Aguirre, L., Hervé, F. & Godoy, E. 1972. Distribution of metamorphic facies in Chile—an outline. *Kristalinikum*, **9**, 7–19.

Alarcón, M., Oliveros, V. & Creixell, C. 2015. Condiciones de metamorfismo de una cuenca de antearco paleozoica a los 29°S, Regiones de Atacama y Coquimbo, Chile. *XV Congreso Geológico Chileno, La Serena*, **1**, 1–4.

Alvarez, J., Mpodozis, C., *et al.* 2011. Detrital zircons from late Paleozoic accretionary complexes in north–central Chile (28°–32°S): Possible fingerprints of the Chilenia terrane. *Journal of South American Earth Sciences*, **32**, 460–472.

Augustsson, C., Rüsing, T., Niemeyer, H., Kooijman, E., Berndt, K., Bahlburg, H. & Zimermann, U. 2015. 0.3 b.y. of drainage stability along the Palaeozoic palaeo Pacific Gondwana margin; a detrital zircon study. *Journal of the Geological Society, London*, **172**, 186–200, http://doi.org/10.1144/jgs2014-065.

Bahlburg, H. & Hervé, F. 1997. Geodynamic evolution and tectonostratigraphic terranes of northwestern Argentina and northern Chile. *Geological Society of America Bulletin*, **109**, 869–884.

Bahlburg, H., Vervoort, J., du Frane, J.S., Bock, B., Augustsson, C. & Reimann, C. 2009. Timing of crust formation and recycling in accretionary orogens: Insights learned from the western margin of South America. *Earth-Science Reviews*, **97**, 227–253.

Baldwin, S.L., Harrison, T.M. & Fitzgerald, J.D. 1990. Diffusion of ^{40}Ar in metamorphic hornblende. *Contributions to Mineralogy and Petrology*, **105**, 691–703.

Berg, K. & Charrier, R. 1987. The rio Choapa transect: A magmatic profile across the Chilean Andes at 31°30′–32°S. *In*: *Symposium on Circum-Pacific Phanerozoic Granites, X Congreso Geológico Argentino, Tucumán, Argentina*, **2**, 11–14.

Cawood, P.A., Hawkesworth, C.J. & Dhuime, B. 2012. Detrital zircon record and tectonic setting. *Geology*, **40**, 875–878.

Cloos, M. & Schreve, R. 1988. Subduction-channel model of prism accretion, mélange formation, sediment subduction, and subduction erosion at convergent plate margins: 1. Background and description. *Pure and Applied Geophysics*, **128**, 455–500.

Creixell, C., Ortiz, M. & Arévalo, C. 2012. *Geología del área Carrizalillo–El Tofo, Regiones de Atacama y Coquimbo, 1:100,000 scale map.* Carta Geológica de Chile, Serie Geología Básica, **133–134**. Servicio Nacional de Geología y Minería, Santiago.

Dahlquist, J.A. & Pankhurst, R.J. *et al.*, 2013. Hf and Nd isotopes in Early Ordovician to Early Carboniferous granites as monitors of crustal growth in the Proto-Andean margin of Gondwana. *Gondwana Research*, **23**, 1617–1630.

Dalla Salda, L.H., Cingolani, C.A. & Varela, R. 1992. Early Paleozoic orogenic belt of the Andes in southeastern South America: result of Laurentia–Gondwana collision? *Geology*, **20**, 617–620.

Davis, J.S., Roeske, S.M., McClelland, W.M. & Kay, S.M. 2000. Mafic and ultramafic crustal fragments of the SW Precordillera terrane and their bearing on tectonic models of the early Paleozoic in W Argentina. *Geology*, **28**, 171–174.

Deckart, K., Hervé, F., Fanning, M., Ramirez, V., Calderon, M. & Godoy, E. 2014. U–Pb geochronology and Hf–O isotopes of zircons from Pennsylvanian coastal batholiths, south–central Chile. *Andean Geology*, **41**, 49–82.

Ernst, W.G. 1975. Systematics of large-scale tectonics and age progressions in Alpine and Circum-Pacific blueschist belts. *Tectonophysics*, **26**, 229–246.

Fisher, D.M. 1996. Fabrics and veins in the forearc: A record of cyclic fluid flow at depths of <15 km. *In*: Platt, J.P. (ed.) *Subduction Top to Bottom.* American Geophysical Union, Geophysical Monographs, **96**, 75–89.

Fleck, R., Sutter, J. & Elliot, D. 1977. Interpretation of discordant ^{40}Ar/^{39}Ar age-spectra of Mesozoic tholeiites from Antarctica. *Geochimica et Cosmochimica Acta*, **41**, 15–32.

García-Sansegundo, J., Farias, P., Heredia, N., Gallastegui, G., Charrier, R., Rubio-Ordoñez, R. & Cuesta, A. 2014. Structure of the Andean Palaeozoic basement in the Chilean coast at 31°30′S: Geodynamic evolution of a subduction margin. *Journal of Iberian Geology*, **40**, 293–308.

Gehrels, G.E., Valencia, V.A. & Ruiz, J. 2008. Enhanced precision, accuracy, efficiency, and spatial resolution of U/Pb ages by laser ablation multicollector inductively coupled plasma mass spectrometry. *Geochemistry, Geophysics, Geosystems*, **9**, Q03017, http://doi.org/10.1029/2007GC001805.

Glodny, J., Lohrmann, J., Echtler, H., Gräfe, K., Seifert, W., Collao, S. & Figueroa, O. 2005. Internal dynamics of a paleoaccretionary wedge: insights from combined isotope tectonochronology and sandbox modelling of the South–Central Chilean forearc. *Earth and Planetary Science Letters*, **231**, 23–39.

Godoy, E. 1985. Nuevos antecedentes sobre el basamento metamórfico y la fase tectónica infraneocomiana en la costa del Norte Chico, Chile. *IV Congreso Geológico Chileno*, **1**, I370–I384.

Godoy, E. & Lara, L. 1998. *Hojas Chañaral y Diego de Almagro, Región de Atacama. Mapas Geológicos, No. 5–6, mapa escala 1:100.000.* Servicio Nacional de Geología y Minería, Santiago.

Godoy, E. & Navarro, J. 2014. Sobre la parte oculta del plutonismo carbonífero-pérmico al oeste de la Cordillera Principal de Chile central. *XIX Congreso Geológico Argentino, Córdoba, S22, Tectónica Andina*, **28**.

Heredia, N., Charrier, R., Farias, P., García-Sansegundo, J., Giacosa, R. & Giambiagi, L. & Paleoandes Group 2014. Evolución geodinámica de los Andes (28°–39°S) durante el Paleozoico. *XIX Congreso Geológico Argentino*, S21–S22.

Hervé, F. 1977. Petrology of the crystalline basement of the Nahuelbuta mountains, south central Chile. *In*: Ishikawa, T. & Aguirre, L. (eds) *Comparative Studies on the Geology of the CircumPacific Orogenic Belt in Japan and Chile.* Japanese Society for the Promotion of Sciences, 1–51.

Hervé, F. 1988. Late Paleozoic subduction and accretion in Southern Chile. *Episodes*, **11**, 183–188.

Hervé, F., Faundez, V., Calderón, M., Massone, H.-J. & Willner, A.P. 2007. Metamorphic and plutonic basement complexes. *In*: Moreno, T. & Gibbons, W. (eds) *The Geology of Chile.* Geological Society, London, 5–19.

Hervé, F., Fanning, M., Calderón, M. & Mpodozis, C. 2014. Early Permian to Late Triassic batholiths of the Chilean Frontal Cordillera (28°–31°S): SHRIMP U–Pb zircon ages and Lu–Hf and O isotope systematics. *Lithos*, **184–187**, 436–446.

Hunziker, J.C., Desmons, J. & Hurford, A.J. 1992. Thirty-two years of geochronological research in the Central and Western Alps: a review on seven maps. *Mémoires de Géologie*, **13**, 1–59.

Hyppolito, T., García-Casco, A., Juliani, C., Meira, V.T. & Hall, C. 2014. Late Paleozoic onset of subduction and exhumation at the western margin of Gondwana (Chilenia Terrane): Counterclockwise *P–T* paths and timing of metamorphism of deep-seated garnet–mica schist and amphibolite of Punta Sirena, Coastal Accretionary Complex, central Chile (34°S). *Lithos*, **206–207**, 409–434.

Kato, T. & Godoy, E. 2015. Middle to Late Triassic mélange exhumation along a pre-Andean transpressional fault system: coastal Chile (26°–42°S). *International Geology Review*, http://doi.org/10.1080/00206814.2014.1002119.

Kato, T., Sharp, W. & Godoy, E. 2008. Inception of a Devonian subduction zone along the southwestern Gondwana margin: ^{40}Ar/^{39}Ar dating of eclogite–amphibolite assemblage in blueschist boulders from the Coastal Range of Chile (41°S). *Canadian Journal of Earth Sciences*, **45**, 337–351.

Lucassen, F., Trumbull, R., Franz, G., Creixell, C., Vásquez, P., Romer, R.L. & Figueroa, O. 2004. Distinguishing crustal recycling and juvenile additions at active continental margins: the Paleozoic to Recent compositional evolution of the Chilean Pacific margin (36–41°S). *Journal of South American Earth Sciences*, **17**, 103–119.

Ludwig, K.R. 2003. *User's manual for Isoplot 3.00: A geochronological toolkit for Microsoft Excel.* Berkeley Geochronological Center Special Publication, **4**.

Maksaev, V., Munizaga, F. & Tassinari, C. 2014. Timing of the magmatism of the paleo-Pacific border of Gondwana: U–Pb geochronology of Late Paleozoic to Early Mesozoic igneous rocks of the north Chilean Andes between 20° and 31°S. *Andean Geology*, **41**, 447–506.

Massonne, H.-J. & Calderón, M. 2008. *P–T* evolution of metapelites from the Guarguaraz Complex, Argentina: evidence for Devonian crustal thickening close to the western Gondwana margin. *Revista Geológica de Chile*, **35**, 215–232.

Miller, C., McDowell, S.M. & Mapes, R. 2003. Hot and cold granites? Implications of zircon saturation temperatures and preservation of inheritance. *Geology*, **31**, 529–532.

Moore, J., Rowe, Ch. & Meneghini, F. 2007. How can accretionary prisms elucidate seismogenesis in subduction zones? *In*: Dixon, T. (ed.) *Proceedings from the Seismogenic Zone Theoretical Institute. Columbia University Press, Snowbird, UT, March 2003*. Columbia University Press, New York, NY, 288–315.

Moscoso, R. 1979. *Geología de la franja transversal a la Cordillera de la Costa y Cordillera de Los Andes a la latitud de Domeyko (29°S), región de Atacama*. Undergraduate Thesis, Universidad de Chile, Santiago.

Mosher, D.C., Austin, J.A., Jr, Fisher, D. & Gulick, S.P.S. 2008. Deformation of the northern Sumatra accretionary prism from high-resolution seismic reflection profiles and ROV observations. *Marine Geology*, **252**, 89–99.

Mpodozis, C. & Kay, S.M. 1992. Late Paleozoic to Triassic evolution of the Gondwana margin: evidence from Chilean Frontal Cordilleran batholiths (28°S to 31°S). *Geological Society of America Bulletin*, **104**, 999–1014.

Mpodozis, C. & Ramos, V.A. 1989. The Andes of Chile and Argentina. *In*: Ericksen, G.E., Cañas Pinochet, M.T. & Reinemud, J.A. (eds) *Geology of the Andes and its Relation to Hydrocarbon and Mineral Resources.* Circumpacific Council for Energy and Mineral Resources, Earth Sciences Series, **11**, 59–90.

Navarro, J. 2013. *Petrotectónica del Complejo Metamórfico Punta de Choros, III–IV Región*. Undergraduate Thesis, Universidad de Chile, Santiago.

Parada, M. 1990. Granitoid plutonism in central Chile and its geodynamic implications; a review. *In*: Kay, S.M. & Rapela, C.W. (eds.) *Plutonism from Antarctica to Alaska*. Geological Society of America, Special Papers, **241**, 51–66.

Passchier, C.W. & Trouw, R.A. 2005. *Microtectonics.* Springer, Berlin.

Peacock, S. 1996. Thermal and petrologic structure of subduction zones. *In*: Platt, J.P. (ed.) *Subduction Top to Bottom.* American Geophysical Union, Geophysical Monographs, **96**, 119–134.

Perchuk, A., Philippot, P., Erdmer, P. & Fialin, M. 1999. Rates of thermal equilibration at the onset of subduction deduced from diffusion modeling of eclogite garnets, Yukon–Tanana terrane, Canada. *Geology*, **27**, 531–534.

Rebolledo, S. & Charrier, R. 1994. Evolución del basamento Paleozoico en el área de Punta Claditas, Región de Coquimbo, Chile (31–32°S). *Revista Geológica de Chile*, **21**, 55–69.

Renne, P.R., Swisher, C.C., Deino, A.L., Karner, D.B., Owens, T.L. & DePaolo, D.J. 1998. Intercalibration of standards, absolute ages and uncertainties in $^{40}Ar/^{39}Ar$ dating. *Chemical Geology*, **145**, 117–152.

Salazar, E., Coloma, F. & Creixell, C. 2013. *Geología del área El Tránsito–Lagunillas, región de Atacama.* Carta Geológica de Chile, Serie Geología Básica, **149**. Servicio Nacional de Geología y Minería, Santiago.

SERNAGEOMIN 2002. Mapa Geológico de Chile, scale 1:1,000,000. *Servicio Nacional de Geología y Minería*, Santiago.

Stacey, J.S. & Kramers, J.D. 1975. Approximation of terrestrial lead isotope evolution by a two-stage model. *Earth and Planetary Science Letters*, **26**, 207–221.

Steiger, R.H. & Jäger, E. 1977. Subcommission on geochronology: convention on the use of decay constants in geo- and cosmochronology. *Earth and Planetary Science Letters*, **36**, 359–362.

Stern, R.J., 2002, Subduction zones. *Reviews of Geophysics*, **40**, 1012, 3-1 - 3-38.

Thiele, R. & Hervé, F. 1984. Sedimentación y tectónica de antearco en los terrenos preandinos del Norte Chico, Chile. *Revista Geológica de Chile*, **22**, 61–75.

Welkner, D., Arévalo, C. & Godoy, E. 2006. *Geología del área Freirina–El Morado, Región de Atacama. Carta Geológica de Chile, Serie Geología Básica, No. 100, mapa escala 1:100.000.* Servicio Nacional de Geología y Minería, Santiago.

Willner, A.P., Glodny, J., Gerya, T.V., Godoy, E. & Massone, H.J. 2004. A counterclockwise *PTt* path of high-pressure/low-temperature rocks from the Coastal Cordillera accretionary complex of south–central Chile: constraints for the earliest stage of subduction mass flow. *Lithos*, **75**, 283–310.

Willner, A.P., Thomson, S.N., Kröner, A., Wartho, J.-A., Wijbrans, J.R. & Hervé, F. 2005. Time markers for the evolution and exhumation history of a Late Palaeozoic paired metamorphic belt in north–central Chile (34°–35°3′S). *Journal of Petrology*, **46**, 1835–1858.

Willner, A.P., Gerdes, A. & Massone, H.-J. 2008. History of crustal growth and recycling at the Pacific convergent margin of South America at latitudes 29°–36°S revealed by a U–Pb and Lu–Hf isotope study of detrital zircon from late Paleozoic accretionary systems. *Chemical Geology*, **253**, 114–129.

Willner, A.P., Gerdes, A., Massone, H.-J., Schmidt, A., Sudo, M., Thomson, S. & Vujovich, G. 2011. The geodynamics of collision of a microplate (Chilenia) in Devonian times deduced by the pressure–temperature–time evolution within part of a collisional belt (Guarguaraz Complex, W Argentina). *Contributions to Mineralogy and Petrology*, **162**, 303–327.

Willner, A., Massone, H.-J., Ring, U., Sudo, M. & Thomson, S. 2012. *P–T* evolution and timing of a late Palaeozoic forearc system and its heterogeneous Mesozoic overprint in north–central Chile (latitudes 31–32°S). *Geological Magazine*, **149**, 177–207.